A conservative phase-field model for reactive transport

C. Bringedal

UHasselt Computational Mathematics Preprint
Nr. UP-19-17

Dec. 24, 2019

A conservative phase-field model for reactive transport

Carina Bringedal

Abstract We present a phase-field model for single-phase flow and reactive transport where ions take part in mineral precipitation/dissolution reactions. The evolving interface between fluid and mineral is approximated by a diffuse interface, which is modeled using an Allen-Cahn equation. As the original Allen-Cahn equation is not conservative, we apply a reformulation ensuring conservation of the phase-field variable and address the sharp-interface limit of the reformulated model. This model is implemented using a finite volume scheme and the discrete conservation of the reformulated Allen-Cahn equation is shown. Numerical examples show how the discrete phase-field variable is conserved up to the chemical reaction.

Key words: Allen-Cahn, Reactive transport, Discrete conservation

MSC (2010)**:** 76D05, 74N20, 65M08

1 Introduction

We consider single-phase flow with solute transport, where ions can form a mineral and hence leave the fluid phase. Also, minerals in the mineral phase can dissolve, releasing ions to the fluid phase. We account for the time evolution of the mineral and fluid phases. This evolution is not known a-priori as it depends on the considered reactions, hence we obtain a free-boundary problem. In [11], existence and uniqueness of a weak solution for such a free-boundary model is proved in a one-dimensional domain. In [9] a free-boundary model for precipitation and dissolution

Carina Bringedal
Stuttgart Center for Simulation Technology (SimTech)
Institute for Modelling Hydraulic and Environmental Systems (IWS)
University of Stuttgart, Pfaffenwaldring 5a, 70569 Stuttgart, Germany
and Computational Mathematics (CMAT), Hasselt University, Belgium
e-mail: carina.bringedal@iws.uni-stuttgart.de

is included in a two-dimensional strip where the mineral width uniquely describes the geometry. A level-set formulation is used for a more general geometry in [8].

These approaches apply a sharp interface between the mineral and fluid. Alternatively, the transition between mineral and fluid can be considered as diffuse. Diffuse-interface models for reactive and diffusive transport have been formulated and analyzed in [10, 12], and later extended to fluid flow in [2]. In these papers the original Allen-Cahn equation [1] describes the evolution of the diffuse interface.

The Allen-Cahn equation is derived from mean-curvature flow. It fulfills the max/min principle, but is in its original form not conservative in the sense that the volume of the considered phases will not remain constant. When using the Allen-Cahn equation to track the location of the mineral and fluid phases, the amount of mineral and fluid is not conserved - also in the absence of chemical reactions. Reformulations to ensure conservation of the phases has been suggested and analyzed in the form of a nonlocal term or a Lagrange multiplier [4, 7, 13]. We will here consider a similar reformulation.

The structure of the paper is as following: In Section 2 we present the original phase-field model from [2] that we will build upon, while in Section 3 the conservative reformulation and its sharp-interface limit is addressed. Section 4 formulates a finite volume scheme and we show that the reformulated Allen-Cahn equation is discretely conservative. Finally we show some numerical examples in Section 5.

2 The original phase-field model and its sharp-interface limit

The original model, as formulated in [2] is, for $\mathbf{x} \in \Omega$, $t > 0$:

$$\lambda^2 \partial_t \phi + \gamma P'(\phi) = \gamma \lambda^2 \nabla^2 \phi - 4\lambda \phi(1-\phi)\frac{1}{u^*} f(u), \tag{1a}$$

$$\nabla \cdot (\phi \mathbf{v}) = 0, \tag{1b}$$

$$\rho_f \partial_t (\phi \mathbf{v}) + \rho_f \nabla \cdot (\phi \mathbf{v} \otimes \mathbf{v}) = -\phi \nabla p + \mu_f \phi \nabla^2 (\phi \mathbf{v}) - \frac{1}{\lambda} g(\phi)\mathbf{v} + \frac{1}{2}\rho_f \mathbf{v} \partial_t \phi. \tag{1c}$$

$$\partial_t \big(\phi(u-u^*)\big) + \nabla \cdot (\phi \mathbf{v} u) = D \nabla \cdot (\phi \nabla u). \tag{1d}$$

Here, Ω is the combined fluid and mineral domain and hence constant in time. The phase field ϕ approaches 1 in the fluid and 0 in the mineral while λ denotes the width of the diffuse zone separating the two phases. The double-well potential is $P(\phi) = 8\phi^2(1-\phi)^2$ and γ is the diffusivity of the interface. Further, $\mathbf{v}$ is the fluid velocity and p the pressure, while ρ_f and μ_f are the constant fluid density and viscosity. Since the flow equations are solved also for the mineral part of the domain, the monotonously decreasing interpolation term $g(\phi)$ fulfilling $g(1) = 0$ and $g(0) > 0$ is included to ensure zero flow in the mineral. The solute concentration is denoted as u, D is its diffusivity, and the constant mineral concentration is u^*. The mineral precipitation and dissolution reaction rate is $f(u) = k(u^2/u_{\text{eq}}^2 - 1)$, where u_{eq} is a given equilibrium concentration and k a reaction constant.

The sharp-interface limit of the model (1) is derived by matched asymptotic expansions in [2]. The background of this procedure can be found in [3]. We let $\Omega_f(t)$ denote the domain where $\phi \to 1$ and $\Omega_g(t)$ where $\phi \to 0$ as $\lambda \to 0$. By separating between these two regions, the model (1) reduces to

$$\nabla \cdot \mathbf{v} = 0 \qquad \text{in } \Omega_f(t), \tag{2a}$$

$$\rho_f \partial_t \mathbf{v} + \rho_f \nabla \cdot (\mathbf{v} \otimes \mathbf{v}) + \nabla p = \mu_f \nabla^2 \mathbf{v} \qquad \text{in } \Omega_f(t), \tag{2b}$$

$$\partial_t u + \nabla \cdot (\mathbf{v} u) = D \nabla^2 u \qquad \text{in } \Omega_f(t), \tag{2c}$$

$$\mathbf{v} = \mathbf{0}, \qquad \text{in } \Omega_m(t), \tag{2d}$$

as $\lambda \to 0$. Through inner expansions and hence investigating the behavior near the diffuse transition zone, it is found that, as $\lambda \to 0$ [2]:

$$v_n = -\gamma \kappa - \frac{1}{u^*} f(u) \qquad \text{on } \Gamma(t), \tag{3a}$$

$$\mathbf{v} = \mathbf{0} \qquad \text{on } \Gamma(t), \tag{3b}$$

$$v_n (u^* - u) = \mathbf{n} \cdot D \nabla u \qquad \text{on } \Gamma(t), \tag{3c}$$

where v_n is the normal velocity of the interface $\Gamma(t)$ and the curvature κ introduces the curvature-driven motion. The normal vector $\mathbf{n}$ points into the mineral.

However, it is clear from (3a) that the interface evolution is not conservative as the curvature-driven motion will alter the size of the fluid/mineral domains. By applying homogeneous Neumann boundary conditions on $\partial\Omega$ we obtain

$$\frac{\mathrm{d}}{\mathrm{d}t} \int_\Omega \phi \, d\mathbf{x} = \int_\Omega \big(-\frac{1}{\lambda^2} \gamma P'(\phi) - \frac{4}{\lambda} \phi (1-\phi) \frac{1}{u^*} f(u) \big) d\mathbf{x},$$

which is non-zero even without chemical reactions.

3 Conservative phase-field model

We now formulate a conservative phase-field model based on the reformulation considered in [13] for phase separation, where also well-posedness of the reformulation was assessed. We replace the phase-field equation (1a) by

$$\lambda^2 \partial_t \phi + \gamma P'(\phi) = \gamma \lambda^2 \nabla^2 \phi - 4\lambda \phi (1-\phi) \frac{1}{u^*} f(u) + \frac{\gamma}{|\Omega|} \int_\Omega P'(\phi) d\mathbf{x}, \tag{4}$$

where $|\Omega|$ is the size of the considered domain. The equations (1b)-(1d) are left unchanged. The reformulated equation (4) fulfills the global conservation property:

$$\frac{\mathrm{d}}{\mathrm{d}t} \int_\Omega \phi \, d\mathbf{x} = \int_\Omega \big(-\frac{4}{\lambda} \phi (1-\phi) \frac{1}{u^*} f(u) \big) d\mathbf{x}. \tag{5}$$

Now the curvature-driven motion does not affect the total amount of ϕ anymore. Interpreting the integrated phase field as porosity, means that porosity can only change due to the mineral precipitation and dissolution.

We address the sharp-interface limit of the reformulated phase-field equation (4) by following similar steps as in [4], where a conservative Allen-Cahn equation without chemical reactions was addressed. The equation (4) is first split in two equations:

$$\lambda^2 \partial_t \phi + \gamma P'(\phi) = \gamma \lambda^2 \nabla^2 \phi - 4\lambda \phi(1-\phi)\frac{1}{u^*} f(u) + \gamma \lambda \xi(t) \tag{6a}$$

$$\xi(t) = \frac{1}{\lambda}\frac{1}{|\Omega|}\int_\Omega P'(\phi) d\mathbf{x}. \tag{6b}$$

The integral in (6b) is small and will decrease as λ decreases. Hence, it is shown in [4] that $\xi(t) = O(\lambda^0)$ as $\lambda \to 0$. The lowest order terms of the outer expansions of (6a) still lead to ϕ approaching 0 and 1 in the mineral and fluid domains as earlier.

For the inner expansions [3], following steps similar as in [2, 4], we arrive at

$$v_n = -\gamma(\kappa - \overline{\kappa}) - \frac{1}{u^*} f(u) \quad \text{on } \Gamma(t),$$

where $\overline{\kappa}$ is the average curvature along $\Gamma(t)$. This means that the interface normal velocity is still driven by both the chemical reaction and by curvature, but where the curvature-driven movement now fulfills conservation of the phase-field parameter.

4 Conservative numerical discretization

As numerical discretization we apply a standard finite-volume scheme on an admissible mesh $\mathscr{E}$ [5], and forward or backward Euler in time with constant time step size Δt. For each element $K \in \mathscr{E}$, the discretization for the phase-field equation (4) reads

$$\begin{aligned}\lambda^2 |K| \frac{\phi_K^{n+1} - \phi_K^n}{\Delta t} + |K| \gamma P'(\phi_K^\ell) &= \gamma \lambda^2 \sum_{L \in \mathscr{N}(K)} |\sigma_{K,L}| F_{K,L}^\ell \\ -4\lambda |K| \phi_K^\ell (1-\phi_K^\ell) \frac{f(u_K^\ell)}{u^*} + |K| \frac{\gamma}{|\Omega|} &\sum_{J \in \mathscr{E}} |J| P'(\phi_J^\ell),\end{aligned} \tag{7}$$

where $|K|$ is the measure of element K. Further, $\mathscr{N}(K)$ refers to the neighboring elements of K and $|\sigma_{K,L}|$ is the measure of the edge $\sigma_{K,L}$ between element K and a neighbor L. The integral $\int_\Omega P'(\phi) d\mathbf{x}$ is approximated by the sum $\sum_{J \in \mathscr{E}} |J| P'(\phi_J^\ell)$. The superscript ℓ can be either n or $n+1$ depending on whether forward or backward Euler is applied. The fluxes $F_{K,L}^\ell$ approximate the diffusive flux from $\nabla^2 \phi$ and are given by

$$F_{K,L}^\ell = \frac{\phi_L^\ell - \phi_K^\ell}{d_{K,L}}$$

where $d_{K,L}$ is the Euclidean distance between the points $x_K \in K$ and $x_L \in L$. Obviously we have $F^\ell_{K,L} = -F^\ell_{L,K}$ on interior edges. As we will apply homogeneous Neumann boundary conditions for ϕ, $F_\sigma \equiv 0$ for edges $\sigma \in \partial\Omega$.

Theorem 1. *The scheme* (7) *is globally conservative (up to the chemical reaction) under homogeneous Neumann boundary conditions on ϕ when the two terms concerning $P'(\phi)$ are either both solved explicitly or both implicitly.*

Proof. We sum over all $K \in \mathscr{E}$. Since $F^\ell_{K,L} = -F^\ell_{L,K}$ on internal edges and $F_\sigma = 0$ on boundary edges, the contribution from the diffusive flux vanishes. Hence,

$$\sum_{K\in\mathscr{E}} |K|\phi_K^{n+1} = \sum_{K\in\mathscr{E}} |K|\phi_K^n + \frac{\Delta t\gamma}{\lambda^2}\sum_{K\in\mathscr{E}} |K|\Big(\frac{1}{|\Omega|}\sum_{J\in\mathscr{E}} |J|P'(\phi_J^\ell) - P'(\phi_K^\ell)\Big) - \frac{4\Delta t}{\lambda}\sum_{K\in\mathscr{E}} |K|\phi_K^\ell(1-\phi_K^\ell)\frac{f(u_K^\ell)}{u^*}.$$

Since $\sum_{K\in\mathscr{E}} |K|\frac{1}{|\Omega|}\sum_{J\in\mathscr{E}} P'(\phi_J^\ell) = \sum_{J\in\mathscr{E}} |J|P'(\phi_J^\ell)$ as $\sum_{K\in\mathscr{E}} |K| = |\Omega|$, the two terms concerning $P'(\phi)$ cancel each other when they are evaluated at the same time level t^n or t^{n+1}. Hence

$$\sum_{K\in\mathscr{E}} |K|\phi_K^{n+1} = \sum_{K\in\mathscr{E}} |K|\phi_K^n - \frac{4\Delta t}{\lambda}\sum_{K\in\mathscr{E}} |K|\phi_K^\ell(1-\phi_K^\ell)\frac{f(u_K^\ell)}{u^*},$$

which means that the scheme is globally conservative in case of $f(u) = 0$, and the integrated value of ϕ can only change due to the chemical reactions. □

5 Numerical examples

We consider two numerical examples in 2D: In the first the Allen-Cahn equation is applied to a circular mineral, while in the second example we consider also (1b)-(1d), where flow through a channel with a dissolving mineral layer is addressed. Equations (1b)-(1d) are discretized with a FV scheme similar as in (7) with u and p at nodes x_K and velocity on a dual mesh for the edge midpoints. The numerical examples use uniform, rectangular meshes. The meshes fulfill $\max\{\Delta x, \Delta y\} < \lambda/4$ to ensure proper resolution of the diffuse interface. For all presented results we use $\gamma = 1$ and $\lambda = 0.1$, but the results are qualitatively the same for other choices. All non-linear systems of equations are solved iteratively using Newton's method.

5.1 Circular mineral

The unwanted behavior of the non-conservative Allen-Cahn equation is especially visible when considering a circular mineral. The constant (and non-zero) curva-

ture of the diffuse interface zone causes the mineral to shrink without the presence of any chemical reaction. Although this is expected from the standard Allen-Cahn equation, it is not wanted when using a phase field to track the location of a mineral.

We initialize the square $\Omega = [0,1]^2$ with a phase field depicting a mineral of radius 0.4 centered in the middle of the square. Homogeneous Neumann conditions are used on all sides. We use the strategy described in [2] to initialize the phase field. No chemical reactions are included.

Figure 1 shows the integrated phase field over time. In the standard Allen-Cahn model the mineral disappears. For the conservative formulation, the changes in porosity are 5.2×10^{-9} and 4.9×10^{-11} for the explicit and implicit formulation, respectively. The changes for the implicit formulation can be connected to the tolerance of the Newton iterations, while the changes for the explicit are mainly an artifact of the explicit time stepping. For the explicit time-stepping phase-field values above 1 and below 0 was encountered.

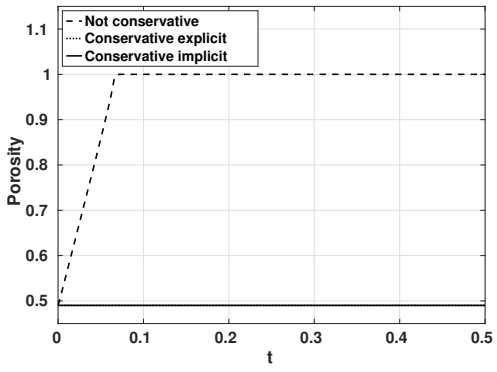

Fig. 1 The integral of the phase field; i.e., porosity, as a function of time. The two lines for conservative implicit and explicit are lying on top of each other.

5.2 Flow through a dissolving channel

We consider a channel $\Omega = [0,1] \times [0,0.1]$ with a prescribed parabolic inflow profile with $v_{\max} = 1$ on the left side and a constant pressure $p = 0$ on the right side. Initially, a mineral layer of width 0.025 is at the top and bottom of the channel, and the fluid is saturated with the equilibrium concentration $u_{\text{eq}} = 0.5$. Due to symmetry we only consider the lower half of the channel. At the left inlet a Dirichlet condition of $u = 0.25$ is applied, triggering mineral dissolution. We consider three cases:

1) The original model (1), solved fully coupled with backward Euler.
2) The conservative model (4), (1b)-(1d), solved fully coupled with backward Euler.
3) The conservative model (4), (1b)-(1d), solved fully coupled with backward Euler except for the two terms concerning $P'(\phi)$, which are both solved explicitly.

The resulting non-linear system of equations is solved with Newton's method. In the second case the Jacobian for the phase-field equation is full and Newton iterations are expensive. Although the third case gives cheaper Newton iterations, a small time-step size is needed to ensure a stable discretization.

In all three cases the mineral dissolves. However, the speed and location of the dissolution vary due to differences in curvature behavior. Figure 2 (left) shows the porosity minus the accumulated reactive term ((5) integrated in time) as function of time for each of the three cases, which should be (close to) zero. Figure 2 (right) shows the across-channel integral of 1-ϕ, giving the mineral width, at $t = 0.3$.

From Figure 2 (left) it is clear that the non-conservative formulation 1) gradually gives an nonphysical porosity due to the curvature-driven motion of the diffuse interface. The conservative implicit formulation 2) only has a nonphysical change in porosity of 6.5×10^{-11} throughout the simulation, which can be connected to the tolerance used for the Newton iterations. Despite applying $\Delta t = 10^{-5}$ for the conservative explicit formulation 3), only solutions up to $t = 0.35$ could be obtained due to instabilities, and a nonphysical change in porosity of 7.9×10^{-8} is observed at this time. The conservative explicit case 3) also shows some difference in curvature behavior compared to case 2) (Figure 2, right). For cases 1) and 3), the mineral dissolves slower near the inlet and faster near the outlet.

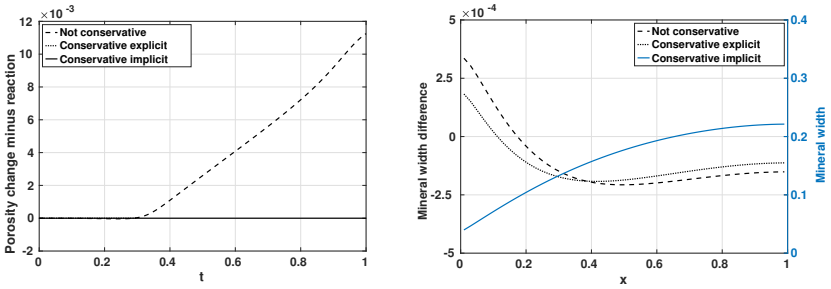

Fig. 2 Left: Changes in porosity not coming from the chemical reaction over time. The dotted line is hidden behind the solid line. Right: Mineral width along the x-axis of case 2) in blue; black lines show difference between case 1) or 3) and 2), at time $t = 0.3$.

6 Discussion and conclusion

We have formulated a conservative phase-field model for flow and reactive transport with a mineral precipitation and dissolution reaction. The sharp-interface limit of the model shows how the interface evolution still includes curvature-driven motion as well as reaction-driven motion, but where the curvature-driven motion is now conservative.

A standard FV scheme on an admissible mesh ensures the discrete conservation of the phase-field variable (up to the chemical reaction) as long as a consistent explicit/implicit choice is made for the non-linear terms. However, the explicit choice needs a very short time step to avoid numerical instabilities to develop. For the implicit choice, the strong nonlinearity in the discretized system of equations creates difficulties and Newton's method is slow due to the Jacobian being full. It would be beneficial to rather use an iterative scheme like the L-scheme [6] to speed up the non-linear solving steps.

Finally, we note that the reformulated phase-field model can be upscaled similarly as in [2], hence a two-scale (pore-Darcy) model can be obtained, where the phase field is updated locally on the pore scale. This way, the conservative property would be achieved for each local pore.

Acknowledgements The author would like to thank Florian Frank (FAU Erlangen-Nürnberg) for useful discussions on the phase-field formulation. The computational resources and services used in this work were provided by the VSC (Flemish Supercomputer Center), funded by the Research Foundation - Flanders (FWO) and the Flemish Government - department EWI.

References

1. Allen, S.M., Cahn, J.W.: A microscopic theory for antiphase boundary motion and its application to antiphase domain coarsening. Acta Metall **27**(6), 1085 – 1095 (1979). DOI 10.1016/0001-6160(79)90196-2
2. Bringedal, C., von Wolff, L., Pop, I.S.: Phase field modeling of precipitation and dissolution processes in porous media: Upscaling and numerical experiments (2019). Preprint, available at http://www.uhasselt.be/Documents/CMAT/Preprints/2019/UP1901.pdf
3. Caginalp, G., Fife, P.: Dynamics of layered interfaces arising from phase boundaries. SIAM J Appl Math **48**(3), 506–518 (1988). DOI 10.1137/0148029
4. Chen, X., Hilhorst, D., Logak, E.: Mass conserving Allen-Cahn equation and volume preserving mean curvature flow. Interface Free Bound **12**, 527549 (2010). DOI 10.4171/IFB/244
5. Eymard, R., Gallouët, T., Herbin, R.: Finite volume methods, vol. 7. Elsevier (2000)
6. List, F., Radu, F.A.: A study on iterative methods for solving Richards' equation. Computat Geosci **20**(2), 341–353 (2016). DOI 10.1007/s10596-016-9566-3
7. Mu, X., Frank, F., Riviere, B., Alpak, F.O., Chapman, W.G.: Mass-conserved density gradient theory model for nucleation process. Ind Eng Chem Res **57**(48), 16,476–16,485 (2018). DOI 10.1021/acs.iecr.8b03389
8. van Noorden, T.L.: Crystal precipitation and dissolution in a porous medium: effective equations and numerical experiments. Multiscale Model Sim **7**(3), 1220–1236 (2009)
9. van Noorden, T.L.: Crystal precipitation and dissolution in a thin strip. Eur J Appl Math **20**(1), 6991 (2009). DOI 10.1017/S0956792508007651
10. van Noorden, T.L., Eck, C.: Phase field approximation of a kinetic moving-boundary problem modelling dissolution and precipitation. Interface Free Bound **13**(1), 29–55 (2011). DOI 10.4171/IFB/247
11. van Noorden, T.L., Pop, I.S.: A Stefan problem modelling crystal dissolution and precipitation. IMA J Appl Math **73**(2), 393–411 (2008). DOI 10.1093/imamat/hxm060
12. Redeker, M., Rohde, C., Pop, I.S.: Upscaling of a tri-phase phase-field model for precipitation in porous media. IMA J Appl Math **81**(5), 898–939 (2016). DOI 10.1093/imamat/hxw023
13. Rubinstein, J., Sternberg, P.: Nonlocal reaction-diffusion equations and nucleation. IMA J Appl Math **48**(3), 249–264 (1992). DOI 10.1093/imamat/48.3.249

UHASSELT

UHasselt Computational Mathematics Preprint Series

2019

UP-19-17 *C. Bringedal*, **A conservative phase-field model for reactive transport**, 2019

UP-19-16 *D. Landa-Marbán, G. Bødtker, B.F. Vik, P. Pettersson, I.S. Pop, K. Kumar, F.A. Radu*, **Mathematical Modeling, Laboratory Experiments, and Sensitivity Analysis of Bioplug Technology at Darcy Scale**, 2019

UP-19-15 *D. Illiano, I.S. Pop, F.A. Radu*, **An efficient numerical scheme for fully coupled flow and reactive transport in variably saturated porous media including dynamic capillary effects**, 2019

UP-19-14 *S.B. Lunowa, I.S. Pop, and B. Koren*, **A Linear Domain Decomposition Method for Non-Equilibrium Two-Phase Flow Models**, 2019

UP-19-13 *C. Engwer, I.S. Pop, T. Wick*, **Dynamic and weighted stabilizations of the L-scheme applied to a phase-field model for fracture propagation**, 2019

UP-19-12 *M. Gahn*, **Singular limit for quasi-linear diffusive transport through a thin heterogeneous layer**, 2019

UP-19-11 *M. Gahn, W. Jäger, M. Neuss-Radu*, **Correctors and error estimates for reaction-diffusion processes through thin heterogeneous layers in case of homogenized equations with interface diffusion**, 2019

UP-19-10 *V. Kučera, M. Lukáčová-Medvidová, S. Noelle, J. Schütz,*, **Asymptotic properties of a class of linearly implicit schemes for weakly compressible Euler equations**, 2019

UP-19-09 *D. Seal, J. Schütz*, **An asymptotic preserving semi-implicit multiderivative solver**, 2019

UP-19-08 *H. Hajibeygi, M. Bastidas Olivares, M. HosseiniMehr, I.S. Pop, M.F. Wheeler*, **A benchmark study of the multiscale and homogenization methods for fully implicit multiphase ow simulations with adaptive dynamic mesh (ADM)**, 2019

UP-19-07 *J.W. Both, I.S. Pop, I. Yotov*, **Global existence of a weak solution to unsaturated poroelasticity**, 2019

UP-19-06 *K. Mitra, T. Köppl, I.S. Pop, C.J. van Duijn, R. Helmig*, **Fronts in two-phase porous flow problems: effects of hysteresis and dynamic capillarity**, 2019

UP-19-05 *D. Illiano, I.S. Pop, F.A. Radu*, **Iterative schemes for surfactant transport in porous media**, 2019

UP-19-04 *M. Bastidas, C. Bringedal, I.S. Pop, F.A. Radu*, **Adaptive numerical homogenization of nonlinear diffusion problems**, 2019

UP-19-03 *K. Kumar, F. List, I.S. Pop, F.A. Radu*, **Formal upscaling and numerical validation of fractured flow models for Richards' equation**, 2019

UP-19-02 *M.A. Endo Kokubun, A. Muntean, F.A. Radu, K. Kumar, I.S. Pop, E. Keilegavlen, K. Spildo*, **A pore-scale study of transport of inertial particles by water in porous media**, 2019

UP-19-01 *Carina Bringedal, Lars von Wolff, and Iuliu Sorin Pop*, **Phase field modeling of precipitation and dissolution processes in porous media: Upscaling and numerical experiments**, 2019

2018

UP-18-09 *David Landa-Marbán, Gunhild Bodtker, Kundan Kumar, Iuliu Sorin Pop, Florin Adrian Radu*, **An upscaled model for permeable biofilm in a thin channel and tube**, 2018

UP-18-08 *Vo Anh Khoa, Le Thi Phuong Ngoc, Nguyen Thanh Long*, **Existence, blow-up and exponential decay of solutions for a porous-elastic system with damping and source terms**, 2018

UP-18-07 *Vo Anh Khoa, Tran The Hung, Daniel Lesnic*, **Uniqueness result for an age-dependent reaction-diffusion problem**, 2018

UP-18-06 *Koondanibha Mitra, Iuliu Sorin Pop*, **A modified L-Scheme to solve nonlinear diffusion problems**, 2018

UP-18-05 *David Landa-Marban, Na Liu, Iuliu Sorin Pop, Kundan Kumar, Per Pettersson, Gunhild Bodtker, Tormod Skauge, Florin A. Radu*, **A pore-scale model for permeable biofilm: numerical simulations and laboratory experiments**, 2018

UP-18-04 *Florian List, Kundan Kumar, Iuliu Sorin Pop and Florin A. Radu*, **Rigorous upscaling of unsaturated flow in fractured porous media**, 2018

UP-18-03 *Koondanibha Mitra, Hans van Duijn*, **Wetting fronts in unsaturated porous media: the combined case of hysteresis and dynamic capillary**, 2018

UP-18-02 *Xiulei Cao, Koondanibha Mitra*, **Error estimates for a mixed finite element discretization of a two-phase porous media flow model with dynamic capillarity**, 2018

UP-18-01 *Klaus Kaiser, Jonas Zeifang, Jochen Schütz, Andrea Beck and Claus-Dieter Munz*, **Comparison of different splitting techniques for the isentropic Euler equations**, 2018

2017

UP-17-12 *Carina Bringedal, Tor Eldevik, Øystein Skagseth and Michael A. Spall*, **Structure and forcing of observed exchanges across the Greenland-Scotland Ridge**, 2017

UP-17-11 *Jakub Wiktor Both, Kundan Kumar, Jan Martin Nordbotten, Iuliu Sorin Pop and Florin Adrian Radu*, **Linear iterative schemes for doubly degenerate parabolic equations**, 2017

UP-17-10 *Carina Bringedal and Kundan Kumar*, **Effective behavior near clogging in upscaled equations for non-isothermal reactive porous media flow**, 2017

UP-17-09 *Alexander Jaust, Balthasar Reuter, Vadym Aizinger, Jochen Schütz and Peter Knabner*, **FESTUNG: A MATLAB / GNU Octave toolbox for the discontinuous Galerkin method. Part III: Hybridized discontinuous Galerkin (HDG) formulation**, 2017

UP-17-08 *David Seus, Koondanibha Mitra, Iuliu Sorin Pop, Florin Adrian Radu and Christian Rohde*, **A linear domain decomposition method for partially saturated flow in porous media**, 2017

UP-17-07 *Klaus Kaiser and Jochen Schütz*, **Asymptotic Error Analysis of an IMEX Runge-Kutta method**, 2017

UP-17-06 *Hans van Duijn, Koondanibha Mitra and Iuliu Sorin Pop*, **Travelling wave solutions for the Richards equation incorporating non-equilibrium effects in the capillarity pressure**, 2017

UP-17-05 *Hans van Duijn and Koondanibha Mitra*, **Hysteresis and Horizontal Redistribution in Porous Media**, 2017

UP-17-04 *Jonas Zeifang, Klaus Kaiser, Andrea Beck, Jochen Schütz and Claus-Dieter Munz*, **Efficient high-order discontinuous Galerkin computations of low Mach number flows**, 2017

UP-17-03 *Maikel Bosschaert, Sebastiaan Janssens and Yuri Kuznetsov*, **Switching to nonhyperbolic cycles from codim-2 bifurcations of equilibria in DDEs**, 2017

UP-17-02 *Jochen Schütz, David C. Seal and Alexander Jaust*, **Implicit multiderivative collocation solvers for linear partial differential equations with discontinuous Galerkin spatial discretizations**, 2017

UP-17-01 *Alexander Jaust and Jochen Schütz*, **General linear methods for time-dependent PDEs**, 2017

2016

UP-16-06 *Klaus Kaiser and Jochen Schütz*, **A high-order method for weakly compressible flows**, 2016

UP-16-05 *Stefan Karpinski, Iuliu Sorin Pop, Florin A. Radu*, **A hierarchical scale separation approach for the hybridized discontinuous Galerkin method**, 2016

UP-16-04 *Florin A. Radu, Kundan Kumar, Jan Martin Nordbotten, Iuliu Sorin Pop*, **Analysis of a linearization scheme for an interior penalty discontinuous Galerkin method for two phase flow in porous media with dynamic capillarity effects** , 2016

UP-16-03 *Sergey Alyaev, Eirik Keilegavlen, Jan Martin Nordbotten, Iuliu Sorin Pop*, **Fractal structures in freezing brine**, 2016

UP-16-02 *Klaus Kaiser, Jochen Schütz, Ruth Schöbel and Sebastian Noelle*, **A new stable splitting for the isentropic Euler equations**, 2016

UP-16-01 *Jochen Schütz and Vadym Aizinger*, **A hierarchical scale separation approach for the hybridized discontinuous Galerkin method**, 2016